JOURNAL OF MATERIALS SCIENCE 18 (1983) 919–929

Internal oxidation in gold alloys containing small amounts of Fe and Sn

HIROKI OHNO, YASUO KANZAWA
Department of Dental Materials Science, School of Dentistry, Higashi-Nippon-Gakuen University, Ishikari-Tobetsu, Hokkaido 061-02, Japan

Internal oxidation was observed in gold-rich alloys as substrates for porcelain veneers in dental restorations, which contain small amounts of Fe and Sn. The internal oxidation proceeded with oxygen ions diffusing to the inner part of the alloy through Fe_2O_3 formed at the grain boundaries of the alloy matrix. SnO_2 was formed internally together with the Fe_2O_3. The external oxidation zone was composed of only Fe_2O_3 in a wide range of Fe and Sn concentrations. Fe_3O_4 was formed with Fe_2O_3 in the Sn-rich composition range by reduction of Fe_2O_3 in the presence of Sn. A band mainly composed of SnO_2 was formed at the inside of the internal oxidation zone in the composition range where Fe_3O_4 formed. In the Sn-rich alloys this internal oxidation band of SnO_2 moved to the external oxidation zone.

1. Introduction

Internal oxidation occurs in alloys with high oxygen solubility when oxygen diffuses into the alloy and reacts with the less noble alloying metal, resulting in a precipitation of oxides of the less noble metal. Various features of internal oxidation have been described by Rhines [1] and Rhines *et al.* [2], Darken [3], Meijering and Druyvesteyn [4], Wagner [5, 6], Rapp and co-workers [7–9], Böhm and Kahlweit [10], Meijering [11], and Klueh and Mullins [12]. In these reports, the theoretical analysis of the precipitation processes of the oxides is based on a uniform diffusion of oxygen into the alloy matrix from the outer surface and ignores inhomogeneities such as grain boundaries, subgrain boundaries, and dislocations. Because of low oxygen solubility no internal oxidation is considered to take place in gold-rich alloys [11].

We have, however, found internal oxidation along the grain boundaries in dental gold alloys for metal–porcelain bonding. The alloys investigated in this paper were oxidized by heating to ~ 1273 K when degassing the alloys and firing dental porcelain. Investigating the oxidation of these alloys is very important because the oxides formed on the alloy surface improves wetting and the adherence between alloy and porcelain and also the oxidized alloy surface, in contact with the fused porcelain, is critical in considering the interface reactions.

Kennedy *et al.* [13] have reported that internal oxidation showed grain-boundary subscaling in nickel–iron alloys. However, in alloys having low oxygen solubility there are no reports that the internal oxidation was affected by the inhomogeneities.

2. Experimental procedure

2.1. Materials

Table I shows the compositions (wt%) of the dental gold alloys used in the experiments. The alloys contained Au (85.5 wt%), Pt, Pd, and Ag as noble metals, and Fe and Sn as base metals. The Fe and Sn content in the alloys totalled 1.5 wt% and the respective amounts were varied in 0.15 wt% increments in the 0 to 1.5 wt% range. All metals used were with a purity better than 99.9%. Weighed amounts of the metals, to give a 10 g sample, were prepared by melting in an argon gas atmosphere. The melting took place in an alumina crucible covered with graphite, heated in a high-frequency induction furnace. Weight loss by the melting was less than 0.02%.

0022–2461/83/030919–11$03.82/0

TABLE I Compositions of the gold alloys in wt%

No.	Au	Pt	Pd	Ag	Fe	Sn
1	85.5	6	6	1	1.50	0
2					1.35	0.15
3					1.20	0.30
4					1.05	0.45
5					0.90	0.60
6					0.75	0.75
7					0.60	0.90
8					0.45	1.05
9					0.30	1.20
10					0.15	1.35
11					0	1.50

2.2. Morphological observations and X-ray microanalysis of the oxidation zone

For morphological observation and X-ray microanalysis of the oxidation zone, the alloys were cast in 3 mm x 3 mm x 10 mm ingots by a dental centrifugal casting machine. The cast specimens were polished metallographically by emery paper and alumina powder and oxidized by heating in an electric furnace at 1273 K for 1 h in air. The oxidized specimens were mounted in very hard metallurgical resin (Epomet, Buehler Co) to prevent rounding of the edges of the specimens. Cross-sections perpendicular to the oxidized surface and cross-sections very close to the oxidized surface ($\sim 1^\circ$ off) were examined. The cross-sections for examination were polished metallographically, and for conductivity a 30 to 40 nm carbon film was vaporized on the polished surface. The oxidation zone on the specimens was examined by scanning electron microscopy and X-ray microanalysis by use of an electron probe X-ray microanalyser (Shimadzu-ARL, type SM, XMA in the following). The acceleration voltage was 25 kV and the sample current was 0.01 μA on the Al_2O_3 standard specimen for the X-ray microanalysis. The detection area of X-ray radiation on the alloy surface was 1 μm ϕ under these analytical conditions.

2.3. Identification of the formed oxides

Plate specimens, 15 mm x 20 mm x 2 mm, were made by casting, polishing, and subsequently oxidizing at 1273 K for 1 h in air in a similar manner to that described above. Identification of oxides formed on the alloy surface was carried out by X-ray diffraction with a diffractometer (Rigaku Denki Co) under the following conditions: Cu target, 35 kV tube voltage and 20 mA current, 2θ scanning speed $1/16^\circ$ min^{-1}, and with $1/2^\circ$, 0.15 mm, $1/2^\circ$ slits. On the basis of the sites of the peaks of radiation intensity, the oxides formed on the alloy surface were identified with the ASTM card index.

3. Results

Figs. 1 to 5 show the XMA results of the sections perpendicular to the oxidized surface. Fig. 1 is obtained from alloy no. 3 containing 1.2 wt% Fe and 0.3 wt% Sn, (a) is the secondary electron image, (b) the X-ray image formed by Au$L\alpha$, (c) that for Sn$L\alpha$, and (d) that for Fe$K\alpha$. The dark areas on the left side of (a) is the resin in which the specimen is mounted. It can be assumed that Fe and Sn are oxidized because O$K\alpha$ radiation was detected in the areas where the two elements are enriched. The X-ray images demonstrate that an external oxidation zone composed of Fe-oxide forms uniformly on the alloy surface, and particles composed of the Fe and Sn oxide exhibit internal oxidation. Granular oxides precipitated deeper into the alloy matrix in the order: alloy no. 2, 3, 4, and deepest, ~ 8 μm, in alloy no. 5.

Fig. 2 shows the secondary electron image (a), and three characteristic X-ray images, (b), (c), and (d), obtained from alloy no. 9 containing 0.3 wt% Fe and 1.2 wt% Sn. Fig. 3 shows the results of a line analysis of Au, Fe, and Sn along the line indicated in Fig. 2a. Despite the low, 0.3 wt%, Fe content the external oxidation zone is composed of Fe-oxide. A layer with low Au content as shown in both Fig. 2b and Fig. 3 indicates a band containing Sn-oxide (2 μm wide) formed by internal oxidation. From alloy no. 5, the granular oxides shown in Fig. 1 stop their inward growth, then gradually spread out, and finally become the band-like structure in Fig. 2.

Fig. 4, obtained from alloy no. 10 containing 0.15 wt% Fe and 1.35 wt% Sn, shows the secondary electron image (a) and X-ray images (b), (c), and (d). The Sn-oxide band appears partly on the alloy surface, indicating external rather than internal oxidation. A transition from internal to external Sn oxidation with increasing Sn content is apparent when comparing the Au$L\alpha$ X-ray images in Fig. 2b with Fig. 4b.

Fig. 5, obtained from alloy no. 11 containing only Sn as base metal, shows the secondary electron image (a), and two X-ray images (b) and (c), demonstrating the oxidation zone of Sn-oxide to be exclusively external.

Figs. 6 and 7 show the results of XMA on the

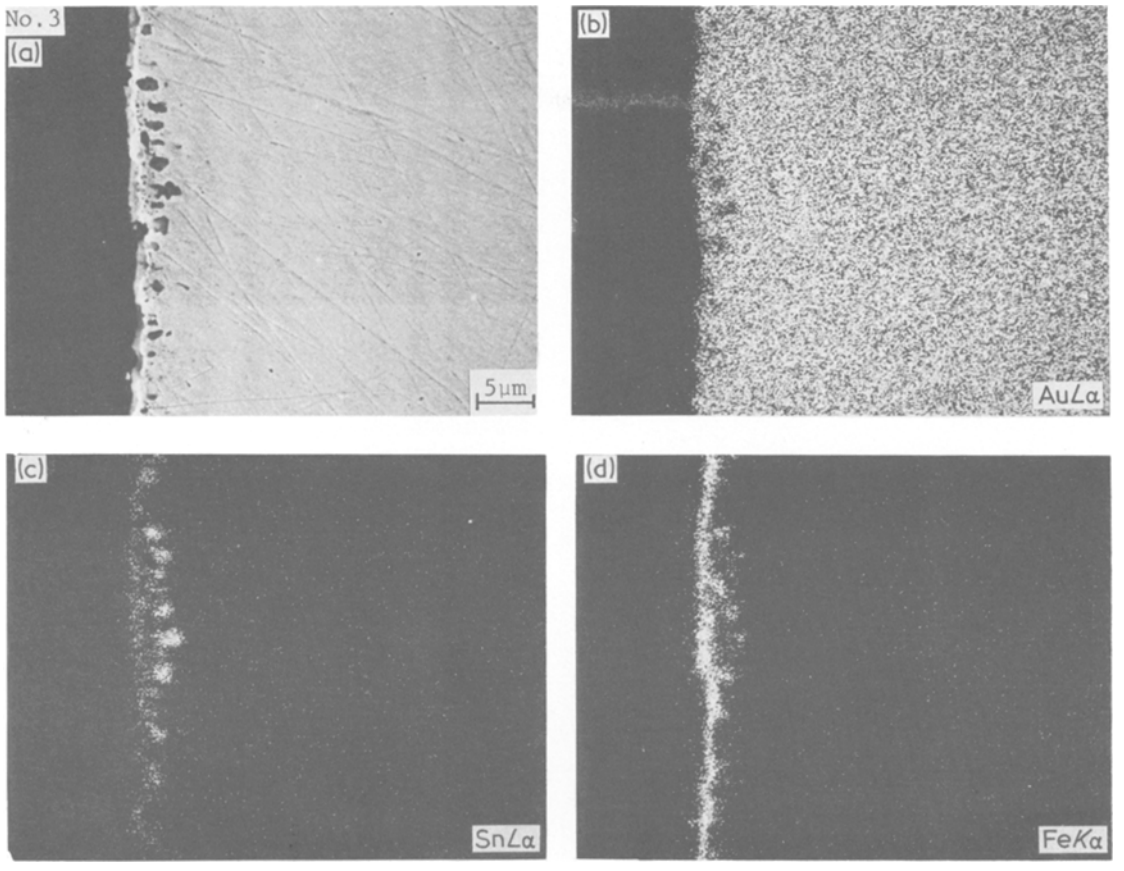

Figure 1 Secondary electron image of cross-section perpendicular to the oxidized surface of alloy no. 3 (a), and characteristic X-ray images of the same area by Au$L\alpha$ (b), Sn$L\alpha$ (c), and Fe$K\alpha$ (d).

cross-section at $\sim 1^\circ$ to the oxidized surface. Fig. 6, obtained from alloy no. 3, shows the secondary electron image (a), and X-ray image (b) formed by Sn$L\alpha$, and (c) formed by Fe$K\alpha$ from the upper (internal oxidation) part of (a). Traces of grain boundaries are clearly shown in both the external and internal oxidation zones (a). The metal grain sizes were confirmed by observation of an unoxidized specimen in a light microscope after metallurgical polishing and chemical etching. The X-ray images, (b) and (c), indicate precipitation of Sn and Fe oxide along the grain boundaries. Very small oxide particles precipitate in the alloy matrix down to 1 μm under the external oxidation zone, but not below 1 μm. Fig. 7, obtained from alloy no. 9, shows the secondary electron image (a) and X-ray images, (b), (c), and (d) formed by Au$L\alpha$, Sn$L\alpha$, and Fe$K\alpha$. Characteristic X-rays are also detected from the resin substrate shown in the bottom of (a) because the resin is very thin. The Fe-oxides distribute uniformly near the surface, while the Sn-oxide precipitates along grain boundaries and connects to form the band observed in Fig. 2. The external oxidation zone in Fig. 3 is not clearly distinguishable.

Fig. 8 represents X-ray powder diffraction patterns obtained from alloy no. 3. Diffraction pattern (a) is from the oxidized alloy surface and (b) is from the internal oxidation zone where the external oxidation zone was removed by polishing. The diffraction patterns, (a) and (b), show Fe_2O_3 and SnO_2 crystals, revealing that the grain-boundary precipitations observed in Figs. 1 and 6 are a mixture of both crystals.

Fig. 9a, b, and c show the X-ray diffraction analysis obtained from the oxidized alloy surface of alloys no. 6, 8, and 10. The diffraction lines of the SnO_2 crystals appeared with high intensity in the three alloys, but are not shown in the figure. Diffraction pattern (a) shows only Fe_2O_3 crystals in the Fe-oxide. Patterns (b) and (c) show Fe_3O_4

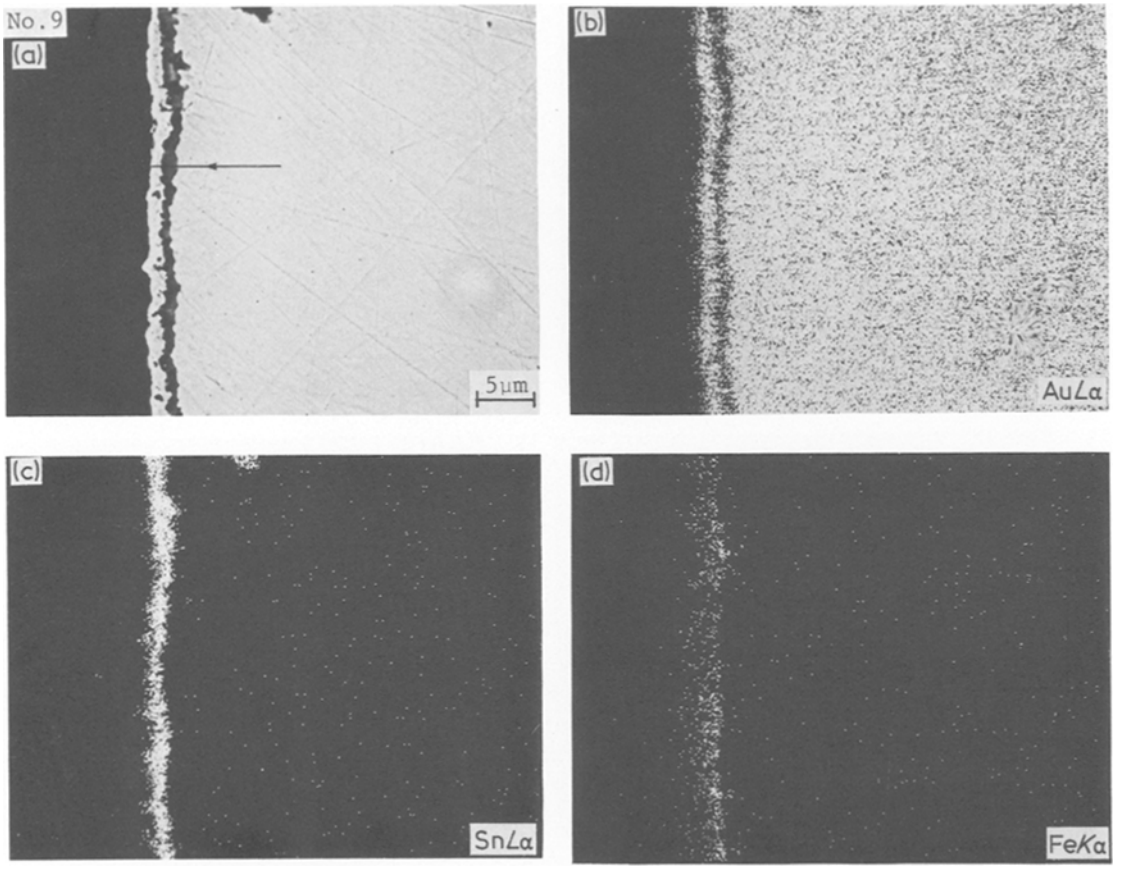

Figure 2 Secondary electron image of cross-section perpendicular to the oxidized surface of alloy no. 9 (a), and characteristic X-ray images of the same area by Au$L\alpha$ (b), Sn$L\alpha$ (c), and Fe$K\alpha$ (d).

in addition to Fe_2O_3. The Fe_3O_4 oxide is formed with increasing Sn concentration and decreasing Fe concentration.

4. Discussion

4.1. Preferential oxidation of Fe

In noble metal alloys containing base metals, the base metal that is oxidized preferentially can be determined by considering the differences between the oxygen activities equilibrating with the oxides and the oxygen activity in the atmosphere [14]. The oxygen activity, $(\mu_O N_O)^v$, which is equilibrated with M_uO_v oxide in Reaction 1 is represented by Equation 2.

$$uM + vO \rightarrow M_uO_v \quad (1)$$

$$(\mu_O N_O)^v = (\mu_M N_M)^{-u} \exp\left(\frac{\Delta G_{M_uO_v}}{RT}\right) \quad (2)$$

where μ_O and μ_M are activity coefficients, N_O and N_M the concentrations of oxygen and base metal, $\Delta G_{M_uO_v}$ is Gibbs standard free energy of formation, R the gas constant, and T the absolute temperature. If the oxygen activity in an atmosphere, $(\mu_O N_O)_{atm}$, is constant, the base metal which forms the oxide with the higher $(\mu_O N_O)_{atm} - (\mu_O N_O)^v$ is preferentially oxidized. Therefore, the metal with higher $-\Delta G$, concentration, and metal/oxygen atomic ratio, u/v, is preferentially oxidized in the alloy.

The values of $-\Delta G$ for the oxides of Fe and Sn are shown in Table II [15]. Both the value of $-\Delta G$ and the atomic ratio u/v (SnO_2:1/2, FeO:1) for FeO are higher than for SnO_2. For this reason, an external oxidation zone of Fe-oxides (rather than SnO_2 oxide) are formed on the alloy surface in alloys with a wide Fe concentration range (1.5 to 0.5 wt %).

In an alloy with an adequate supply of Fe atoms Paidassi [16] reports the resulting external oxidation zone as Fe_2O_3 on top, Fe_3O_4 at the centre, and FeO at the alloy/oxide interface and

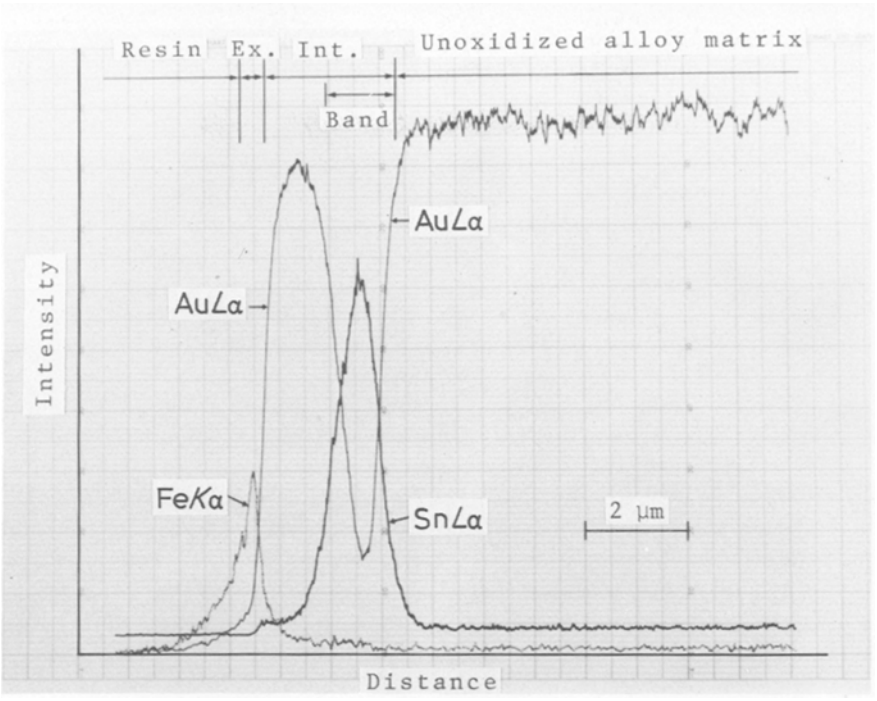

Figure 3 Element analysis by XMA along the line indicated in Fig. 2a. Ex; external oxidation zone, Int; internal oxidation zone.

the thickness of the Fe_2O_3 top layer is very thin, only a few per cent for the total thickness. The gold alloys with high Fe contents in this experiment were almost exclusively covered with Fe_2O_3. In the first stage of oxidation FeO is formed on the surface as explained above, but the reaction rate of oxidation from FeO to Fe_3O_4 and Fe_2O_3 may be much faster than the diffusion of Fe atoms to the alloy surface because the diffusion of Fe atoms is blocked by oxides precipitated at the grain boundaries as discussed below. The result is an external oxidation zone of only Fe_2O_3.

4.2. Internal oxidation in gold alloys

Meijering [11] has listed three conditions for internal oxidation of a solute B in a binary alloy A–B:

(1) the alloy must have appreciable solubility of oxygen;

(2) oxygen must diffuse more rapidly in the solvent A than in the solute B;

(3) the oxygen affinity of element B must be considerably greater than that of element A.

Internal oxidation based on these considerations has been reported by several investigators [2, 4, 6]. The gold alloys investigated here do not satisfy the first and third requirements. The solubility of oxygen would be very small in an alloy containing 85.5 wt % Au, and the SnO_2 was formed in the alloy matrix with low oxygen concentration, and despite Sn having lower affinity for oxygen than Fe.

Therefore, it may be concluded that the mechanism of internal oxidation of the gold alloys in this study is essentially different from oxidation satisfying the three conditions above. The internal oxidation mechanism in the studied gold alloys can be explained on the basis of the property of Fe_2O_3, where O^{2-} diffuse more easily than Fe ions as indicated in Table III. The O^{2-} diffuse by transfering an oxygen vacancy in the Fe_2O_3 crystal [17].

Precipitation of very fine oxide particles down to 1 μm under the external oxidation zone indicates that oxygen permeates uniformly in an extremely thin layer of an alloy matrix with high Au content. Deeper in the alloy matrix, oxygen predominantly diffuses along grain boundaries, as the grain boundary permits a much higher rate of diffusion than the grains. Kofstad gives the diffusivity at the boundary/diffusivity in the grain $\geqq 10^5$ to 10^6 [18]. The oxygen which penetrates through the external Fe_2O_3 layer diffuses along the grain boundaries into the inner part of the alloy.

FeO is first formed at the grain boundary by the reaction of the solute Fe and diffused oxygen.

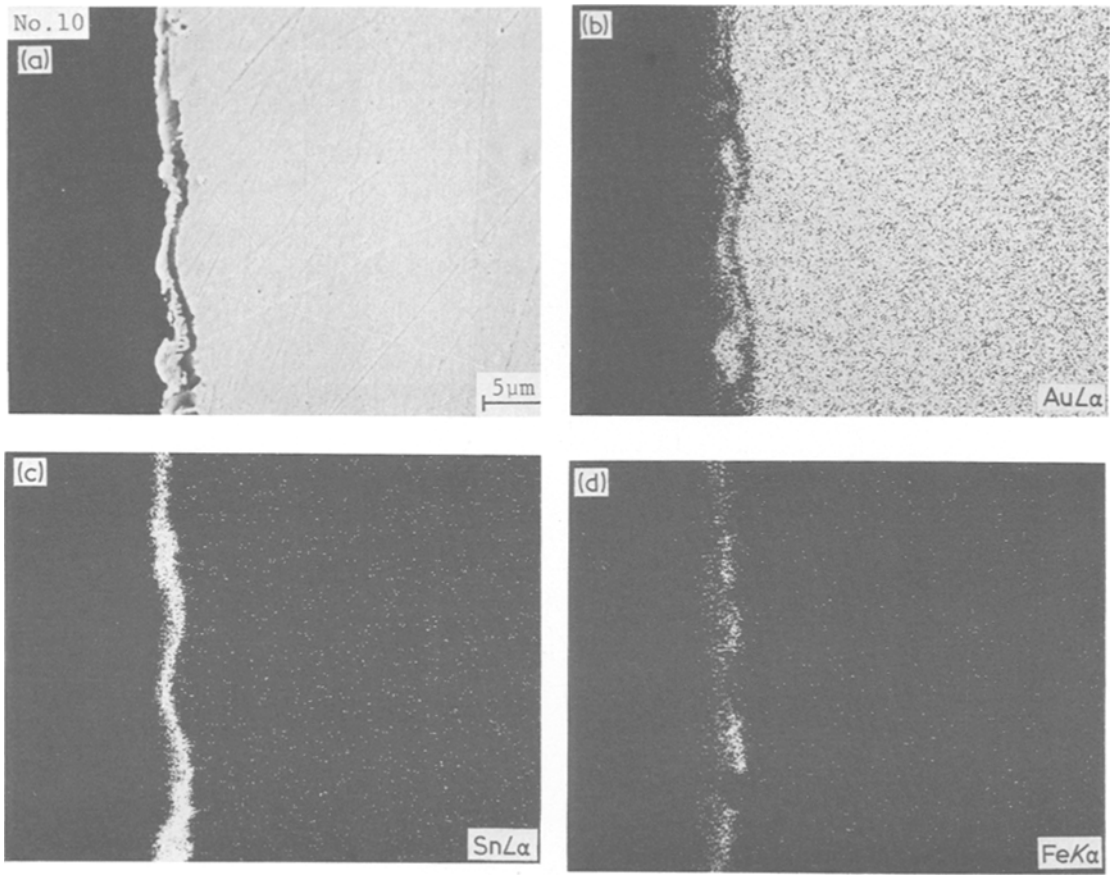

Figure 4 Secondary electron image of cross-section perpendicular to the oxidized surface of alloy no. 10 (a), and characteristic X-ray images of the same area by Au$L\alpha$ (b), Sn$L\alpha$ (c), and Fe$K\alpha$ (d).

If there is no Fe to react with the oxygen, the oxygen reacts with Sn to form SnO_2. A continuous replenishing of oxygen along the grain boundary is effected by the concentration gradient of oxygen, generated by the oxygen consumption. FeO is thermodynamically unstable, and oxidizes to Fe_3O_4 and Fe_2O_3 when Sn concentration is low. As the Fe_2O_3 and SnO_2 do not form a double oxide [19], both oxides precipitate at the grain boundaries. An interface between these oxides may build up an incoherent boundary because of the different crystal systems, Fe_2O_3 (hexagonal, corundum structure) and SnO_2 (tetragonal, rutile structure). Incoherent regions may also be generated at the interface of the oxide and the alloy matrix. Volume increments due to oxidation generate stress in the precipitated region as the Pilling–Bedworth ratios of Fe_2O_3 and SnO_2 are 2.2 and 1.3. Incoherent boundaries and stress may result in regions of lattice mismatch and disorder causing enhanced diffusion [20].

The growth of the external oxidation zone is retarded as the zone becomes thicker and it finally stops growing because the oxide formation along the grain boundaries considerably disturbs diffusion of Fe and Sn atoms from the inner alloy. Owing to the blocked diffusion, the oxides at the grain boundaries do not grow past a certain thickness, and the Fe and Sn atoms contained in a grain contributed to the oxide formation at only its grain boundary. The oxygen diffuses through grain-boundary oxide and incoherent boundaries, and as a result the internal oxidation takes place predominantly along the grain boundaries.

4.3. Formation of an internal oxidation band

Meijering [21] and Rapp [7, 9] have reported that when the oxygen partial pressure is reduced during heating in internal oxidation experiments, the internal oxidation front moves backwards towards the outer surface of the specimen, and a high con-

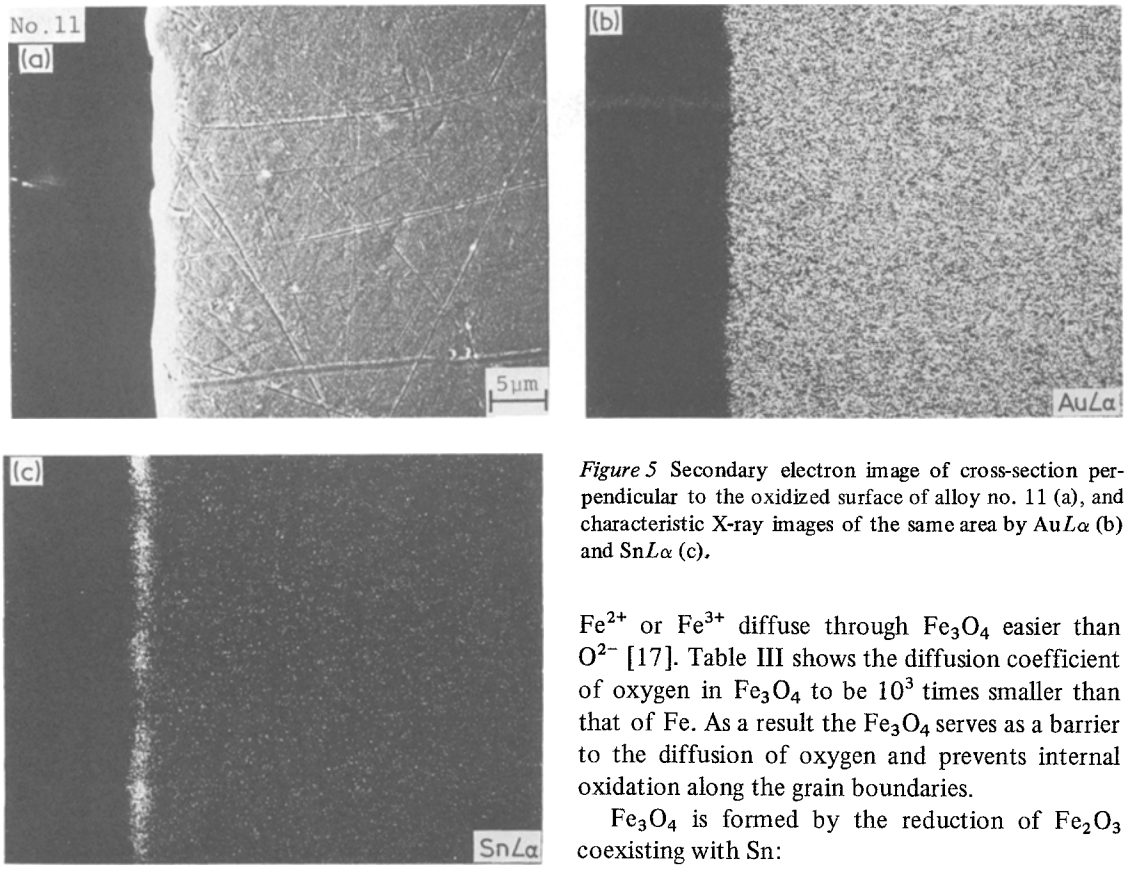

Figure 5 Secondary electron image of cross-section perpendicular to the oxidized surface of alloy no. 11 (a), and characteristic X-ray images of the same area by Au$L\alpha$ (b) and Sn$L\alpha$ (c).

centration band of oxide (interruption band) is formed at the front. The width x_i, of the band has been represented by [7]:

$$x_i = \frac{\xi}{1 + (2N_O D_O / nN_M D_M)} \quad (3)$$

where, ξ is the depth of the internal oxidation zone, N_M the mole fraction of the solute in the alloy, N_O the mole fraction of oxygen at the outer surface of the specimen, and D_M and D_O are the diffusivities of the solute metal and oxygen. For internal oxidation to occur, the rate of diffusion of oxygen in the alloy must be appreciably higher than that of the solute metal. Furthermore, reductions in the oxygen partial pressure as well as increases in solute metal concentration suppress the growth of the internal oxidation zone and results in growth of the oxidation band.

From the above, the formation mechanism of the internal oxidation band observed in alloys no. 9 (Fig. 2) and no. 10 (Fig. 4) with high Sn concentrations can be explained on the basis of the formation of Fe_3O_4 in addition to the Fe_2O_3. Fe^{2+} or Fe^{3+} diffuse through Fe_3O_4 easier than O^{2-} [17]. Table III shows the diffusion coefficient of oxygen in Fe_3O_4 to be 10^3 times smaller than that of Fe. As a result the Fe_3O_4 serves as a barrier to the diffusion of oxygen and prevents internal oxidation along the grain boundaries.

Fe_3O_4 is formed by the reduction of Fe_2O_3 coexisting with Sn:

$$\left.\begin{aligned} 3Fe_2O_3 &\rightarrow 2Fe_3O_4 + O \\ Sn + 2O &\rightarrow SnO_2 \end{aligned}\right\}. \quad (4)$$

The O^{2-} necessary in the formation of the internal oxidation band is both supplied from the atmosphere and released by the reaction. A decrease in the oxygen supply results in a drop in the oxygen partial pressures at the reaction front. An increase in Sn concentration increases the Sn diffusion from the inner part of the alloy to the reaction front more than the O^{2-} supply. In Equation 3, a higher N_M value, caused by an increase in Sn concentration, and a smaller D_O, caused by the formation of Fe_3O_4, give rise to the growth of the internal oxidation band of SnO_2.

A change from an internal oxidation zone to an external one was observed when increasing the Sn content to 1.35 wt% as shown in Fig. 4. Darken [3] has reported that if the concentration of an alloying element is increased above a certain critical value, a transition from internal to external oxidation occurs. Wagner [5] has proposed that the transition is due to blocking of the diffusion paths, caused by the precipitated oxide particles. Precipitation of Fe_2O_3 oxide in the gold alloy

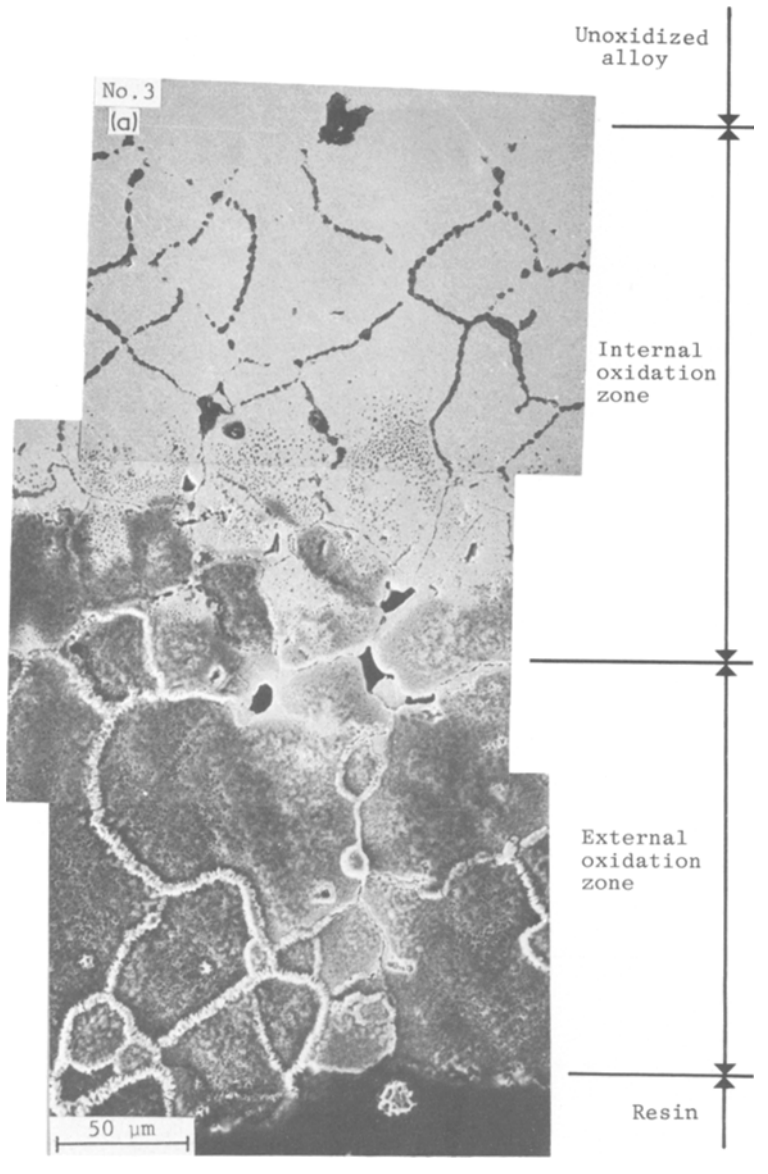

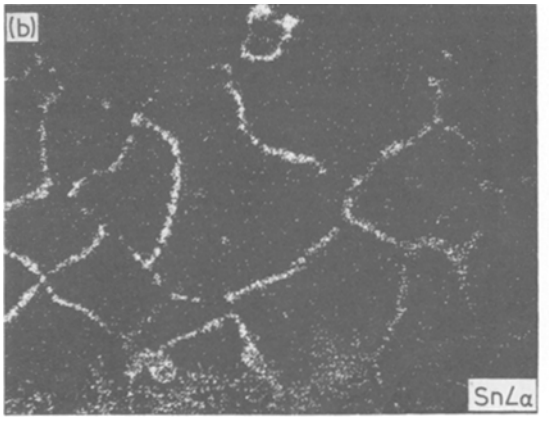

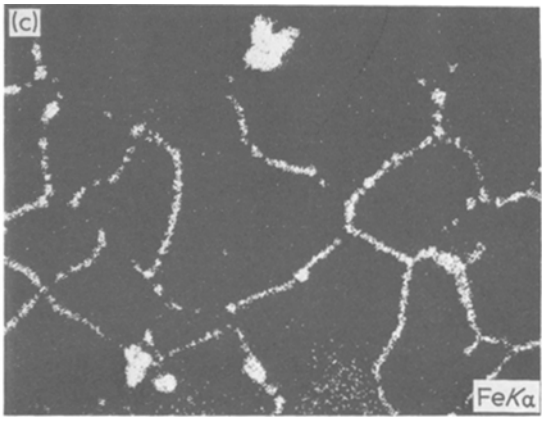

Figure 6 Secondary electron image of cross-section inclined ~ 1° to the oxidized surface of alloy no. 3 (a), and characteristic X-ray images of upper part of (a) by Sn$L\alpha$ (b) and Fe$K\alpha$ (c).

matrix does not block the diffusion of oxygen but serves as a penetration path. In the gold alloys here, the oxygen supply necessary to support internal oxidation is blocked mechanically by the formation of Fe_3O_4 and further controlled by the chemical reduction, $Fe_2O_3 \rightarrow Fe_3O_4 + O$.

5. Conclusions

Internal oxidation zones observed in 85.5 wt % Au–Pt–Pd–Ag alloys containing 1.5 wt % (total) of Fe and Sn oxidized at 1273 K in air were examined by X-ray microanalysis, secondary electron microanalysis, and X-ray diffraction. The

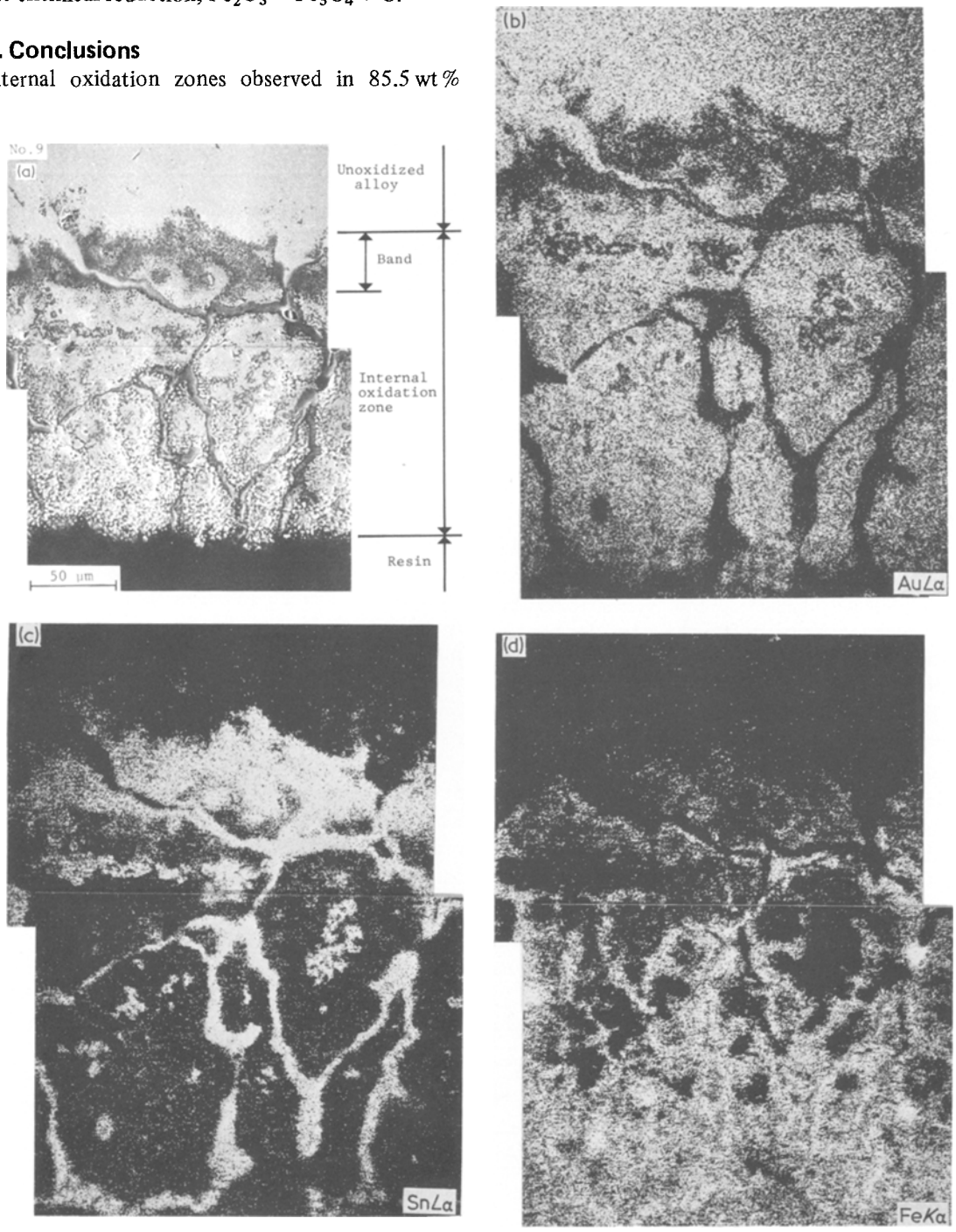

Figure 7 Secondary electron image of cross-section inclined ~ 1° to the oxidized surface of alloy no. 9 (a), and characteristic X-ray images of the same area by Au$L\alpha$ (b), Sn$L\alpha$ (c), and Fe$K\alpha$ (d). The characteristic X-ray are also detected from the substrate of the resin in the lower part of (a).

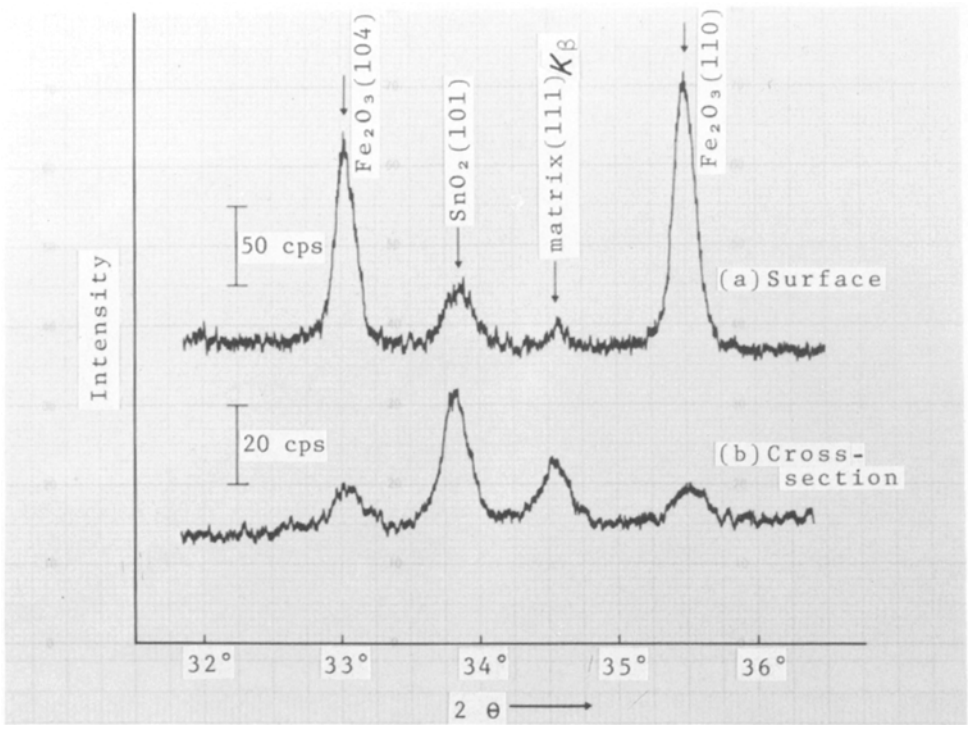

Figure 8 X-ray diffraction patterns obtained from the oxidized surface of alloy no. 3 (a), and cross-section of the internal oxidation zone with the external oxidation zone removed by polishing (b).

morphological changes in the internal oxidation zone accompanying different Fe and Sn concentrations are observed and the formation mechanism is discussed.

High Fe content (1.5 to 0.6 wt % Fe, 0 to 0.9 wt % Sn) leads to the formation of an external oxidation zone composed of Fe_2O_3 and an internal oxidation zone of Fe_2O_3 and SnO_2 precipitated as a network along the grain boundaries. The internal oxidation along the grain boundaries occurs as Fe_2O_3 is preferentially penetrated by O^{2-} rather than Fe ions, and the Fe_2O_3 acts as a diffusion path which permits the penetration of O^{2-} into the alloy. The internal oxidation of Sn occurs when no Fe ions are available.

In the range (0.6 to 0.15 wt % Fe, 0.9 to 1.35 wt % Sn) of low Fe and high Sn content, Fe_2O_3 forms an external oxidation zone and Fe_3O_4 precipitates in the internal oxidation zone, and in addition a band which is mainly composed of SnO_2 is formed on the alloy side of the internal oxidation zone. The Fe_3O_4 is formed by the reduction of the Fe_2O_3 coexisting with Sn. The SnO_2 band may be formed as the supply of Sn is high in comparison to the amount of O^{2-} at the reaction front, because the Fe_3O_4 serves as a barrier to the diffusion of the O^{2-}, the supply of O^{2-} is further controlled by the reduction of Fe_2O_3.

The internal oxidation band partially changed to an external oxidation zone at high Sn contents.

TABLE II Values of Gibbs standard free energy of formation for base metal oxides

Reaction	$-\Delta G$(kJ) at 1273 K [15]
$\{Sn\} + (O_2) = SnO_2$	313.5*
$2\langle Fe\rangle + (O_2) = 2FeO$	363.8
$6\langle FeO\rangle + (O_2) = 2Fe_3O_4$	306.0
$4\langle Fe_3O_4\rangle + (O_2) = 6Fe_2O_3$	140.6

*This value was extrapolated from 1000 K.

TABLE III Diffusion coefficients in oxides

Diffusion substances in oxides	D ($cm^2\,sec^{-1}$)	Temperatures (K)	References
Fe in Fe_3O_4	1.6×10^{-10}	1273	[22]
Fe in Fe_3O_4	3.2×10^{-15}	823	[22]
O in Fe_3O_4	3.9×10^{-18}	823	[23]
Fe in Fe_2O_3	2.5×10^{-14}	1273	[24]
O in Fe_2O_3	5.0×10^{-14}	1273	[25]

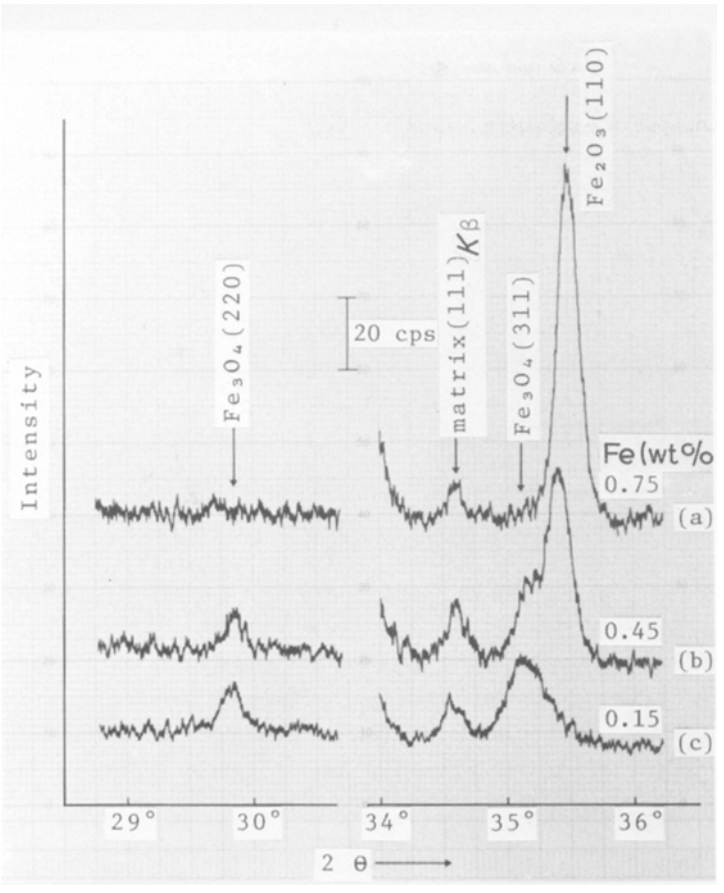

Figure 9 X-ray diffraction patterns obtained from the oxidized surface of alloys no. 6 (a), no. 8 (b), and no. 10 (c).

Acknowledgements

The authors wish to thank Professor K. Nishida and Dr T. Narita for their helpful suggestions, and Professor M. Ohta and Dr S. Ohkawa for the use of the electron probe X-ray microanalyser.

References

1. F. N. RHINES, *Trans. AIME* **137** (1940) 246.
2. F. N. RHINES, W. A. JOHNSON and W. A. ANDERSON, *ibid.* **147** (1942) 205.
3. L. S. DARKEN, *ibid*, **150** (1942) 157.
4. J. L. MEIJERING and M. J. DRUYVESTEYN, *Philips Res. Rept.* **2** (1947) 81, 260.
5. C. WAGNER, *Z. Elektrochem.* **63** (1959) 773.
6. *Idem, J. Colloid. Sci.* **5** (1950) 85.
7. R. A. RAPP, *Acta Metall.* **9** (1961) 730.
8. J. W. ARMITAGE and R. A. RAPP, *Sci. Am. Rev.* **5** (1963) 67.
9. R. A. RAPP, D. F. FRANK and J. V. ARMITAGE, *Acta Metall.* **12** (1964) 505.
10. G. BÖHM and M. KAHLWEIT, *ibid.* **12** (1964) 641.
11. J. L. MEIJERING, *Adv. Met. Res.* **5** (1971) 1.
12. R. L. KLUEH and W. W. MULLINS, *Acta Metall.* **17** (1969) 69.
13. S. W. KENNEDY, L. D. CALVERT and N. COHEN, *Trans. AIME* **215** (1959) 64.
14. T. IGARASHI, M. SHIBATA and Y. KODAMA, *J. Japan Inst. Metals* **44** (1980) 378.
15. O. KUBASHEWSKI and C. B. ALCOCK, "Metallurgical Thermochemistry" (Pergamon Press, New York, 1979) p. 378.
16. J. PAIDASSI, *J. Metals* **4** (1952) 536.
17. K. HAUFFE, "Oxidation of Metals" (Plenum Press, New York, 1965) p. 285.
18. P. KOFSTAD, "High-Temperature Oxidation of Metals" (John Wiley, New York 1966) p. 108.
19. J. CASSEDANNE, *Ann. Acad. Brasil. Cienc.* **38** (1966) 266.
20. S. GOTO and S. KODA, *J. Japan Inst. Metals* **34** (1970) 319.
21. J. L. MEIJERING, *Z. Electrochem.* **63** (1959) 824.
22. S. M. KLOTSMAN, A. N. TIMOFEYEV and I. Sh. TRAKTENVERG, *Phys. Met. Metallogr.* **10** (1960) 93.
23. "Diffusion Data", **2**, 1 (1967–68) p. 48.
24. R. LINDNER, *Arkiv Kemi* **4** (1952) 381.
25. W. C. HAGEL, *Trans. AIME* **236** (1966) 179.

Received 19 May
and accepted 29 July 1982